Available online at www.sciencedirect.com

SciVerse ScienceDirect

Ceramics International 38 (2012) 1195–1204

CERAMICS INTERNATIONAL

www.elsevier.com/locate/ceramint

Fabrication and characterization of ZnO modified bioactive glass nanoparticles

Abeer M. El-Kady [a,c,*], Ashraf F. Ali [b,c]

[a] Biomaterials Department, National Research Center, 33 El-Bohooth St., Dokki 12622, Cairo, Egypt
[b] Inorganic Chemistry Department, National Research Center, 33 El-Bohooth St., Dokki 12622, Cairo, Egypt
[c] Advanced Materials and Nanotechnology Lab., Center of Excellence, National Research Center, Dokki 12622, Cairo, Egypt

Received 6 September 2010; received in revised form 6 June 2011; accepted 24 July 2011
Available online 2 September 2011

Abstract

Bioactive glass nanoparticles in the system (SiO_2–CaO–P_2O_5–ZnO) were synthesized following the sol–gel technique. The prepared glass nanoparticles of 1, 3 and 5 wt% of ZnO (coded: GZ1, GZ3 and GZ5, respectively) were characterized by TEM, FTIR, XRF, TGA and DSC. All glass powders had particle sizes less than 100 nm. Textural analysis revealed that for GZ1, GZ3 and GZ5, the average pore diameters, measured by the high-speed gas sorption analyzer, were 15.9, 15.4 and 15.2 nm, respectively, while the average pore diameters measured by the mercury intrusion porosimetry were 47, 50 and 63 nm, respectively. All glass powders were highly porous (75, 76 and 75%) with surface areas of 233, 94 and 118 m^2/g for GZ1, GZ3 and GZ5, respectively. All glass powders induced an apatite layer on their surfaces upon immersion in simulated body fluid (SBF) as verified by SEM and TF-XRD.

Keywords: *In vitro* bioactivity; Bioactive glass nanoparticles; Sol–gel method; Zinc

1. Introduction

Zinc is an essential trace element that has an important role in bone formation [1]. It is fundamental for bone cell growth and its development and differentiation [2–5]. Zinc is a cofactor for many enzymes. It stimulates protein synthesis and it is essential for DNA replication. Zinc deficiency is associated with skeletal growth retardation and alterations in bone tissue calcification [6]. Recently, zinc-containing ceramics have been developed for bone engineering applications. Zinc-modified calcium silicate ceramics ($Ca_2ZnSi_2O_7$) were shown to support human osteoblast-like cells attachment to a well-organized cytoskeleton structure. They also support an increased cellular proliferation and differentiation with increased expression levels of osteoblast-related mRNAs (alkaline phosphatase, collagen type I, osteocalcin) as compared to calcium silicate ceramics ($CaSiO_3$) [7,8]. Ito et al. [9–11] prepared zinc-containing calcium phosphate ceramics and demonstrated quantitatively that they stimulated bone formation in rabbit femora [12]. This stimulatory effect was ascribed to the zinc ions released from the ceramics. Several studies have provided evidences that ceramics with nanometer grain sizes selectively enhance osteoblast function, leading to more bone growth than materials with micrometer grain size [13,14]. However, the previously reported [15] incorporation of zinc into the structure of bioactive glass particles, following the traditional sol–gel method, has lead to glass particles of micro-scale grain sizes. Therefore, in our current study, to produce zinc-modified glass nanoparticles, a two acid–base catalyzed sol–gel process was followed and a subsequent application of moderate ultrasonic dispersion and mechanical agitation were applied to prevent the formation of a bulk gel during gelation. The glass nanoparticles were characterized and tested for their *in vitro* bioactivity in a simulated body fluid.

2. Materials and methods

2.1. Materials

Tetraethyl orthosilicate (TEOS), calcium nitrate tetrahydrate $Ca(NO)_3{\cdot}4H_2O$, and triethyl phosphate, (TEP), were all ≥98%

* Corresponding author at: Biomaterials Department, National Research Center, 33 El-Bohooth St., Dokki 12622, Cairo, Egypt.
Tel.: +202 333 70933; fax: +202 333 70931.
E-mail address: abeerelkady_2000@yahoo.co.uk (A.M. El-Kady).

0272-8842/$36.00
doi:10.1016/j.ceramint.2011.07.069

and purchased from Fluka (Buchs, Switzerland). Zinc nitrate hexahydrate $Zn(NO_3)_2{\cdot}6H_2O$ was ≥98%, and purchased from Riedel-de Haen). Ammonia solution, 33%, and Nitric acid, 68%, were from Merck, USA. Both nitric acid and ammonia solutions were diluted to 2 M using distilled water.

2.2. Sol–gel synthesis of bioactive glass nanoparticles

Bioactive glass nanoparticles in the system (SiO_2–CaO–P_2O_5–ZnO) were synthesized following a modification of a previously described procedure [16,17]. The formation of the gel was conducted into a conventional ultrasonic bath followed by mechanical agitation to prevent the formation of a bulk gel during gelation. Finally, the prepared gels were dried at 75 °C for 2 days in a drying oven. According to the results obtained from the thermal analysis of the dry gels, which showed that no further weight loss above 700 °C, the gels were stabilized by heat treatment, at a constant heating rate of 3 °C/min up to 700 °C. Table 1 lists the nominal compositions and codes of the prepared glasses.

2.3. Characterization

The morphology and particle sizes of the prepared zinc-containing bioactive glass powder were analyzed using TEM (JEM2010, Japan) working at 200 kV. The elemental compositions of the glasses were determined by energy dispersive X-ray analysis (JEOL JXA-840A, Electron probe micro-analyzer). Thermogravimetric analyses (TGA), and differential calorimetric (DSC) analyses were performed for the dried gels using a computerized 7 series USA PerkinElmer thermal analysis system. Scans were performed in air at a temperature range of 50–1000 °C and a rate of 10 °C/min using aluminum oxide powder as a reference. The infrared spectra of the prepared glasses were recorded in a wave number range of 400–4000 using a Fourier transformer infrared spectrophotometer (FT-IR) (model FT/IR-6100 type A). The quantitative analysis of the composition (wt%) of the glass nanoparticles was measured by X-ray Fluorescence method (PW2404, PHILIPS). The pore volume, average pore diameter in the microporous and mesoporous range, as well as the surface area of the glass nanoparticles were measured with a high-speed gas sorption analyzer (NOVA 2000 series, Chromatic, UK) at 77 K. The porosity%, bulk densities and the average pore diameters in the mesoporous, as well as macroporous range were determined using the mercury intrusion porosimetry technique (19321, Micrometric, USA).

Table 1
Nominal compositions and codes of the prepared zinc containing sol–gel bioactive glasses nanoparticles.

Sample code	Composition (wt%)			
	SiO_2	CaO	P_2O_5	ZnO
GZ1	58	32	9	1
GZ3	58	30	9	3
GZ5	58	28	9	5

2.4. In vitro bioactivity evaluation

The *in vitro* bioactivity of the glasses was assessed by investigating the formation of apatite on their surfaces on immersion in a simulated body fluid (SBF) under normal physiological conditions as proposed by others [18]. Glass disks were prepared and soaked in SBF and maintained at 37 °C for two weeks. The SBF had a composition and an ionic

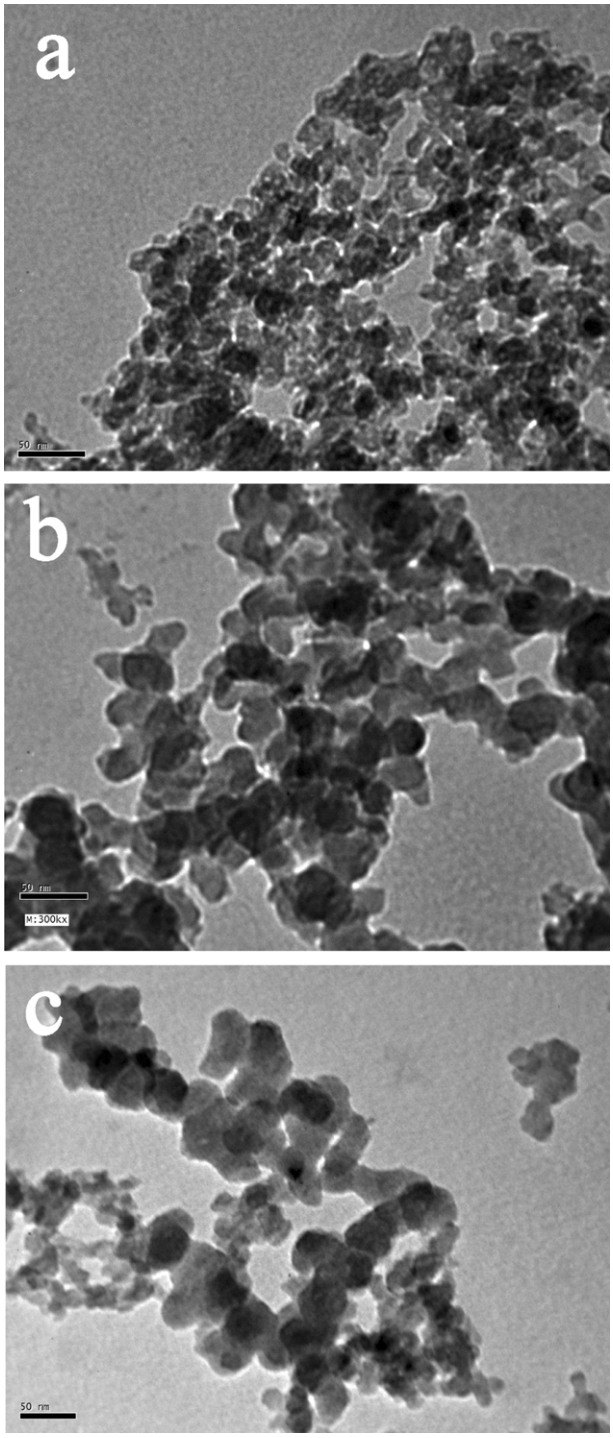

Fig. 1. The TEM micrographs of the prepared glass nanoparticles containing 1, 3 and 5 wt% of zinc oxide samples (GZ1 (a), GZ3 (b), and GZ5 (c), respectively).

concentration almost equal to human plasma. The inorganic ion concentrations in SBF, expressed in mM, were: 142.0, 5.0, 2.5, 1.5, 148.0, 4.2, 1.0, and 0.5 for Na^+, K^+, Ca^{2+}, Mg^{2+}, Cl^-, HCO_3^-, HPO_4^{2-}, SO_4^{2-}, respectively. The solution was buffered at pH 7.4 with tris(hydroxymethyl) aminomethane and 1 M HCl at 37 °C [18]. The formation and growth of apatite layer on the surface of the glass disks were verified by scanning electron microscopy coupled with energy-dispersive spectroscopy, SEM/EDXA (JEOL JXA-840A, Electron probe micro-analyzer, Japan) and thin-film X-ray analysis (TF-XRD) (Panalytical, X'Pert Pro, The Netherlands), employing a Ni-filtered Cu Kα irradiation at 45 kV and 40 mA.

3. Results and discussion

3.1. TEM

Fig. 1 shows the TEM micrographs of the prepared glasses containing 1, 3 and 5 wt% of zinc oxide (GZ1 (a), GZ3 (b), and GZ5 (c) respectively). All glass powders show agglomerated nanoparticles of less than 100 nm size. In most sol–gel procedures to synthesize glasses, the sols are formed by the hydrolysis of low molecular weight alkoxysilanes, such as tetraethoxysilane (TEOS), using water in the presence of a catalyst. In the hydrolysis reaction, the alkoxide groups are replaced with hydroxyl groups. Siloxane bonds (Si–O–Si) are then formed during subsequent condensation. Further condensation leads to gelation which, after drying, forms a dry gel called xerogel [19].

The whole preparation process can be generally described by the following reactions:

$$Si(OCH_3)_4 + nH_2O \rightarrow Si(OCH_3)_{4-n}(OH)_n + nCH_3OH \quad \text{(hydrolysis)} \tag{1}$$

$$-SiOH + CH_3O-Si \rightarrow -Si-O-Si- + CH_3OH \quad \text{(alcohol condensation)} \tag{2}$$

$$-Si-OH + OH-Si- \rightarrow -Si-O-Si- + H_2O \quad \text{(water condensation)} \tag{3}$$

The introduction of calcium ions to the silica network was expressed by the following reaction:

$$Ca^{2+} + 2[Si-OH] \leftrightarrow Si-O\cdots Ca\cdots O-Si + 2H^+ \tag{4}$$

Zinc was incorporated into the glass structure by the following equation

$$Zn^{2+} + 2[Si-OH] \leftrightarrow Si-O\cdots Zn\cdots O-Si + 2H^+ \tag{5}$$

The final size of the sol–gel derived powder depends greatly on the type of the catalysts used, which influences the pH of the solution and alters the relative rates of hydrolysis and condensation reactions [20]. Preparation of bioactive glasses following a one-step acid catalysis requires long gelation times.

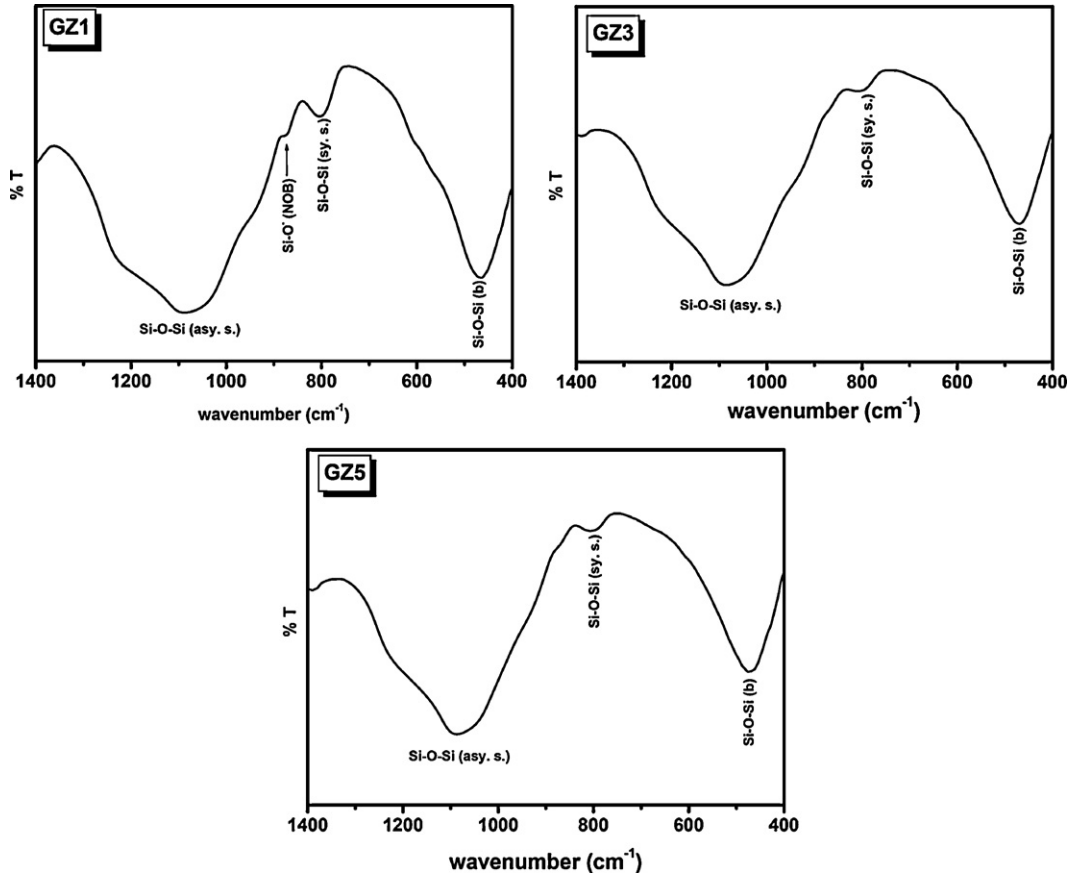

Fig. 2. FTIR spectra of samples GZ1, GZ3 and GZ5.

This allows for the aggregation and growth of colloidal particles in the solution, leading to final products with micro-scale particle sizes [13,21]. However, in this study, a two-step acid–base catalysis was followed. The addition of ammonia solution, as a second catalyst, to a sol that was initially catalyzed by nitric acid was found to increase the rate of condensation and reduce gelation time to few minutes. The condensation rate is proportional to [OH^-] above the isoelectric point [22,23]. In this study, excess 2 M ammonia was used for gelation to provide an environment of a pH much higher than the isoelectric point of silica [23]. Therefore, the gelation time was shortened. In our study, fast gelation of the sols, the application of moderate ultrasonic dispersion combined with mechanical agitation, and the addition of ethanol, as dispersant, prevented the growth of colloid particles during gelation. Therefore, glass particles of less than 100 nm were successfully prepared using the two-step acid–base catalysis.

3.2. FTIR

The FTIR spectra of the GZ1, GZ3 and GZ5 are shown in Fig. 2. For all glass samples, the bands located in the range of 1000–1200 cm^{-1} correspond to the Si–O–Si asymmetric stretching vibration whereas the bands observed in the range of 725–800 cm^{-1} are attributed to the Si–O–S symmetric stretching vibration [24,25]. In addition, the bands located in the range of 450–480 cm^{-1} are ascribed to the [Si–O–Si] bending mode [26]. The very weak peak seen in the FTIR spectrum of GZ1 at 878 cm^{-1}, which was assigned to the Si–O^- of the SiO_4 tetrahedra having two non-bridging oxygen per tetrahedron (Si–O– 2NBO) [25]. This band could not be identified in the spectra of other glass samples. This could be explained by the fact that the backbone of the silicate glass structure was the SiO_4 tetrahedral network in which the SiO_4 tetrahedral were connected only at the oxygen ions at the corners to form a continuous 3D network [27]. Alkali and alkaline earth oxides (Na^+, Ca^{2+}) serve to modify this network structure as they reduce the degree of connectivity in the network by replacing the bridging oxygen (BO) ions, which formed the link between two SiO_4 tetrahedral, by non-bridging oxygen (NBO). On the other hand, previous studies had shown that ZnO could act both as a network modifier and as an intermediate oxide in the glass structure. Data in the literature showed that as the ZnO content was increased, it switched its role from a network modifier to an intermediate oxide [27–29], thus creating a more stable glass structure by forming covalent links between adjacent SiO_4

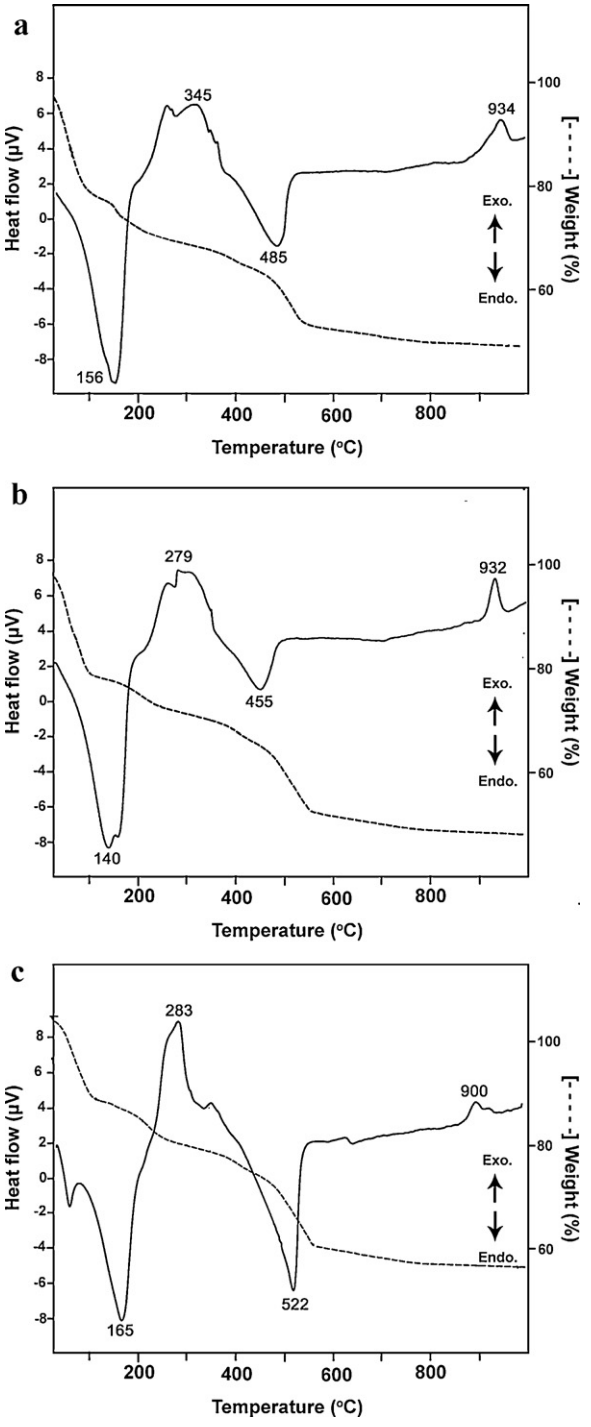

Fig. 3. Thermogravimetric analysis, (TGA), and differential scanning calorimetric (DSC) analysis, curves for samples GZ1, GZ3, and GZ5 (a, b and c, respectively).

Table 2
Quantitative analysis of the composition of zinc incorporated bioactive glasses measured by XRF as compared to the designed compositions.

Constituents	GZ1 (wt%)		GZ3 (wt%)		GZ5 (wt%)	
	Design	Experiment	Design	Experiment	Design	Experiment
SiO_2	58	57.6	58	56.9	58	56.8
CaO	32	32.2	30	29.8	28	27.1
P_2O_5	9	8.6	9	8.7	9	8.5
ZnO	1	0.9	3	2.8	5	5.3
Impurity	–	0.7	–	1.6	–	2.1

Table 3
The data of the textural analysis carried out for GZ1, GZ3 and GZ5.

Sample code	Data measured by high-speed gas sorption analyzer			Data measured by mercury intrusion porosimetry technique		
	Average pore diameter (nm)	Surface area (m^2/g)	Bulk density (g/ml)	Apparent density (g/ml)	Average pore diameter (nm)	Total porosity (%)
GZ1	15.9	233	0.70	2.8	47	75
GZ3	15.4	94	0.72	3.1	50	76
GZ5	15.2	118	0.67	2.7	63	75

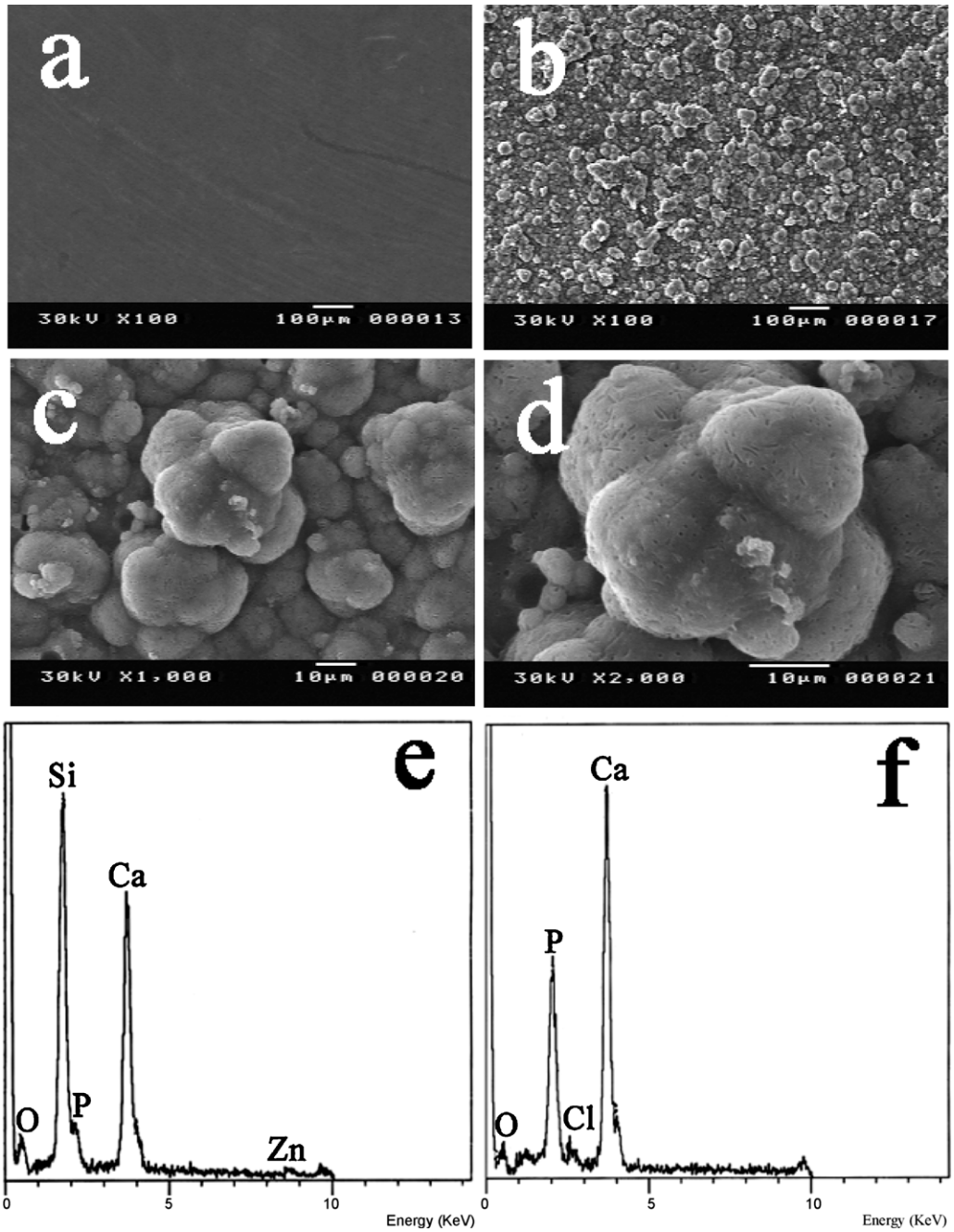

Fig. 4. SEM micrographs of the surface of samples GZ1 before (a) and after (b, c, and d) the immersed in SBF for two weeks. The EDX analysis of the surface before, (e), and after, (f), immersion in SBF are included.

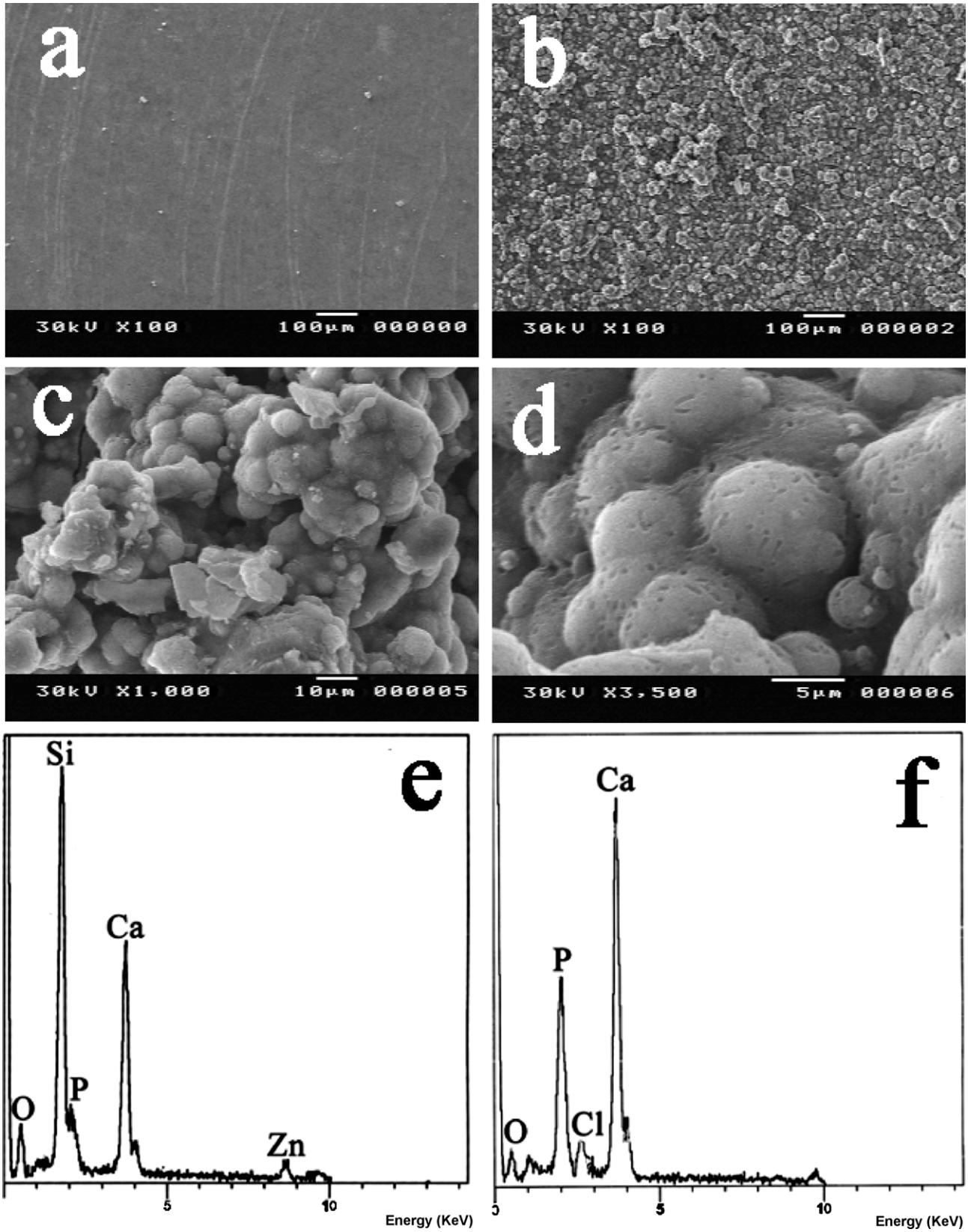

Fig. 5. SEM micrographs of the surface of sample GZ3 before, (a), and after, (b, c, and, d), immersed in SBF for two weeks. The EDX analysis of the surface before, (e), and after, (f), immersion in SBF are included.

tetrahedral and resulting in the creation of bridging species rather than forming non-bridging oxygen. In this study, CaO was replaced by ZnO in the different glass compositions. Hence, the FTIR spectra of the glass samples containing higher zinc contents (GZ3 and GZ5) show no sign of the band at 878 cm^{-1}, which is assigned to $Si–O^-$ with two non bridging oxygen per SiO_4 tetrahedron (Si–O– 2NBO).

3.3. Thermal analysis

Thermogravimetric analysis, (TGA), and differential scanning calorimetric, (DSC), analysis curves for GZ1, GZ3 and GZ5 are shown in Fig. 3 (a, b and c, respectively). The TGA curves of all samples showed three mass losses as the heating process proceeded from room temperature to 1000 °C. Those weight losses appeared at the temperature intervals of 30–170, 170–400, and 400–550 °C for all samples. The first weight loss was attributed to the elimination of residual alcohol and physically adsorbed humidity water from the pores of the gel. This was reflected in the DCS curves of GZ1, GZ3 and GZ5 as the first large endothermic peak centered at around 156, 140 and 165 °C, respectively [16,30]. The second weight loss was reflected in the exothermic peaks centered at around 345, 297 and 283 °C on the DSC curves of GZ1, GZ3 and GZ5, respectively, which was most likely due to desorption of chemically adsorbed water [31]. The third weight loss shown by the TGA curves of all samples was

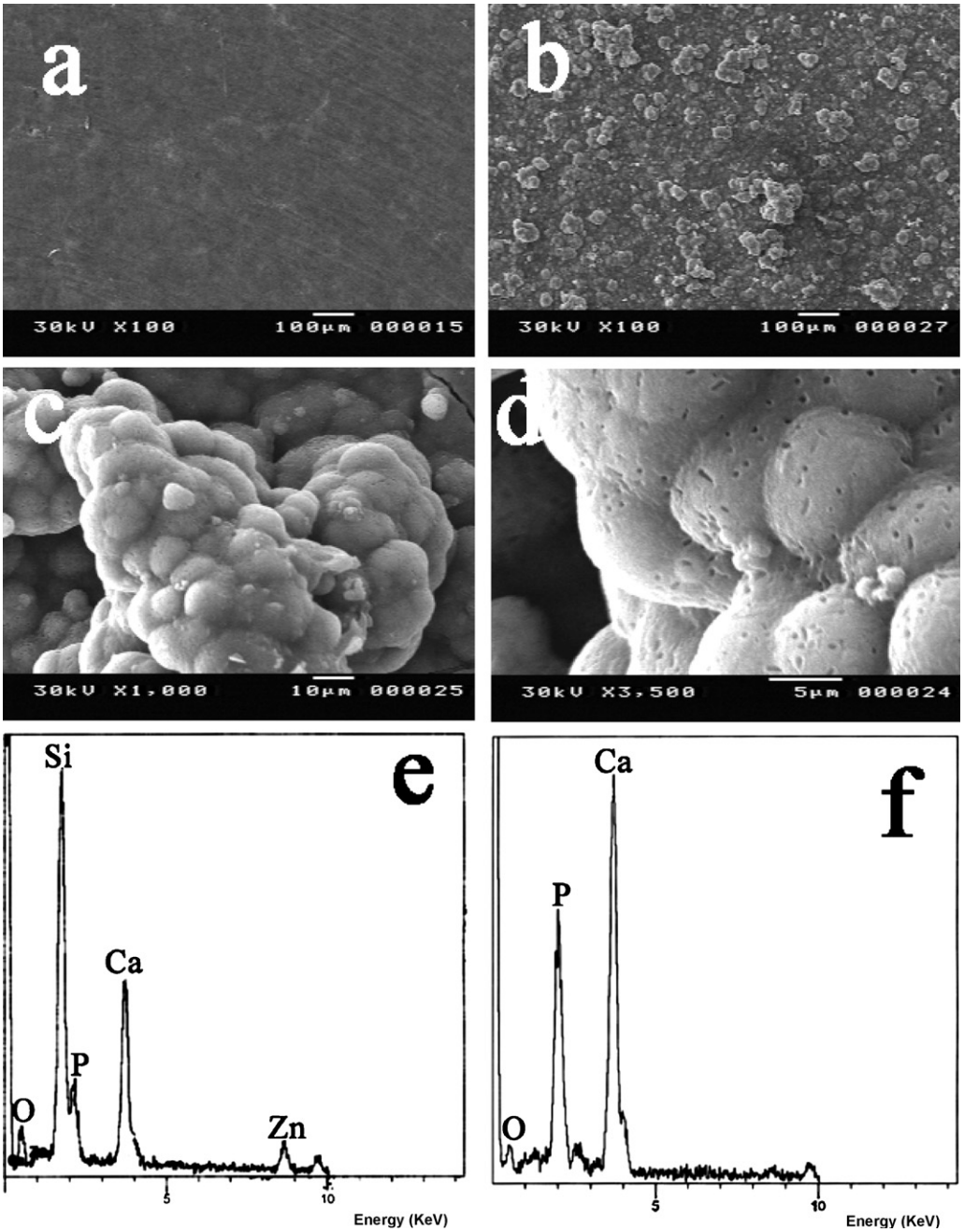

Fig. 6. SEM micrographs of the surface of sample GZ5 before, (a), and after, (b, c, and d), immersed in SBF for two weeks. The EDX analysis of the surface before, (e), and after, (f), immersion in SBF are included.

due to the decomposition of nitrates NO_3^-. The endothermic peaks centered at around 485, 455, and 522 °C on the DSC curves of GZ1, GZ3 and GZ5, respectively, were due to this decomposition. A final, and well-defined, sharp exothermic peak appeared on the DSC curves of all samples and located at 934, 932, and 900 °C, for GZ1, GZ3, and GZ5, respectively. This was due to the glass crystallization into glass-ceramic [32].

3.4. XRF

The quantitative analysis of the compositions, (wt%), of zinc-doped bioactive glasses was measured by XRF, and compared with the designed compositions as shown in Table 2. The results showed that the compositions of the obtained glasses were almost consistent with the designed ones, which indicated that their compositions were not affected by rapid gelation during the synthesis.

3.5. Textural analysis

Table 3 summarizes the data of the textural analysis carried out for glass nanopowders. For samples GZ1, GZ3 and GZ5, the average pore diameters, measured by high-speed gas sorption analyzer, were 15.9, 15.4, and 15.2 nm, respectively, while the

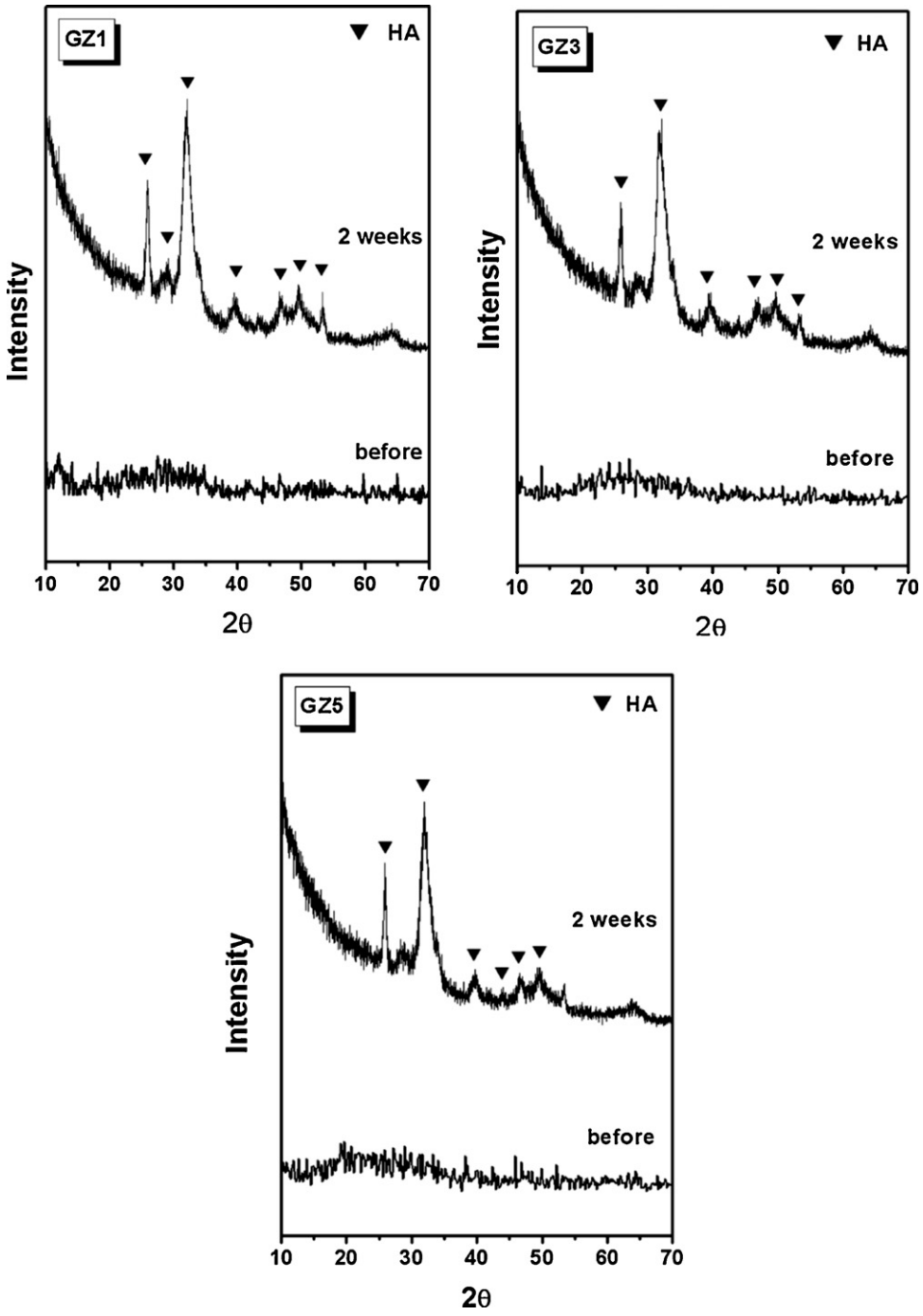

Fig. 7. TF-XRD patterns of glass samples GZ1, GZ3, and GZ5 before and after immersion in the SBF for two weeks.

average pore diameters, measured by mercury intrusion porosimetry technique, were 47, 50 and 63 nm, respectively. The difference in the average pore diameters as measured by the two techniques, is originated from the fact that the high-speed gas sorption analyzer could measure pores in the microporous range, (average pore diameter <2 nm), as well as the mesoporous range, (average pore diameter lying between 2 and 50 nm), while the mercury intrusion porosimetry technique could measure pores in the mesoporous range and the macroporous range (pore diameters greater than 50 nm) range [33]. Textural analysis revealed that GZ1, GZ3 and GZ5 samples had high porosity% values (75, 76, and 75, respectively), and their surface areas were found to be 233, 94, and 118 m^2/g, respectively. The porous nature of those materials originates from the manner by which the gel was formed. The alkoxide precursors reacted with water, and the hydrolyzed species linked together in a condensation reaction. The liquid solvents (water and ethanol) that participated in the process were retained in the capillaries of the structure. The porosity of the glasses was attributed to water and ethanol evaporation, as well as to nitrate decomposition during the stabilization process.

3.6. In vitro bioactivity

3.6.1. SEM

Figs. 4–6 show the SEM micrographs of the surfaces of the samples GZ1, GZ3 and GZ5, respectively, before (a), and after (b–d) their immersion in SBF for two weeks. Before immersion, the surfaces of all glass disks were smooth. After immersion, the micrographs indicated the nucleation and growth of spherical particles that completely covered their surfaces. Moreover, the figures included the EDX analysis of the surfaces of the samples before, (e), and after immersion, (f). Silica, calcium, phosphorous and zinc peaks were observed in the EDX analysis for all samples before immersion. However, after immersion in SBF, the peaks of silica and zinc disappeared and only the peaks of calcium and phosphorous were observed. This indicated the complete covering of the glass surfaces with an apatite layer. For all samples, the EDX analysis of those spherical particles gave Ca/P ratios in the range of 1.69–1.93. Those ratios are similar to that of the natural apatite in bone [34]. For the explanation of the formation of hydroxyapatite layer on the surface of samples, others proposed a complex 5-stage process [35] where exchange of the network modifier calcium with protons, dissolution of soluble silica at the glass solution interface, condensation and re-polymerization of an SiO_2-rich layer on the surface, migration of Ca^{2+} and PO_4^{3-} groups to the surface to form a $CaO–P_2O_5$-rich film, and the eventual growth and crystallization of the amorphous $CaO–P_2O_5$-rich film were the main processes.

3.6.2. TF-XRD

TF-XRD patterns of samples GZ1, GZ3 and GZ5, before and after immersion in the SBF for two weeks, are shown in Fig. 7. Before immersion, the pattern showed the amorphous nature of all glass samples, where no distinct crystalline diffraction patterns were observed. However, after the immersion in the SBF, the typical diffraction pattern of crystalline hydroxyapatite appeared with strong peaks at *d*-spacing values of 2.81, 3.43, and 2.64 Å (matched with ICSD card number 016–742). The appearance of other less intense peaks with d-spacing values of 5.18, 2.27, 1.94, 1.84, and 1.72 Å, (matched with ICSD card number 016-742), was noticed confirming the apatite formation.

4. Conclusion

Sol–gel synthesis and *in vitro* characterization of bioactive glass nanoparticles modified with different zinc contents (1, 3, and 5 wt%) were carried out in this work. All glass samples had particle size of less than 100 nm. Textural analysis revealed that the samples were highly porous and had large surface area. Each sample was able to induce the formation of an apatite layer on its surface upon immersion in SBF which demonstrate their potential application in bone integration.

References

[1] K.B. Hadley, S.M. Newman, J.R. Hunt, Dietary zinc reduces osteoclast resorption activities and increases markers of osteoblast differentiation, matrix maturation, and mineralization in the long bones of growing rats, J. Nutr. Biochem. 21 (2010) 297–303.
[2] M. Yamaguchi, H. Oishi, Y. Suketa, Stimulatory effect of zinc on bone formation in tissue culture, Biochem. Pharmacol. 36 (1987) 4007–4012.
[3] J.R. Popp, B.J. Love, A.S. Goldstein, Effect of soluble zinc on differentiation of osteoprogenitor cells, J. Biomed. Mater. Res. A. 81 (2007) 66–769.
[4] T. Wang, J.C. Zhang, Y. Chen, P.G. Xiao, M.S. Yang, Effect of zinc ion on the osteogenic and adipogenic differentiation of mouse primary bone marrowstromal cells and the adipocytic trans-differentiation of mouse primary osteoblasts, J. Trace Elem. Med. Biol. 21 (2007) 84–91.
[5] M. Yamaguchi, A. Igarashi, S. Ychiyama, Bioavailability of zinc yeast in rats: stimulatory effect on bone calcification in vivo, J. Health Sci. 50 (2004) 75–81.
[6] W.R. Holloway, F.M. Collier, R.E. Herbst, J.M. Hodge, G.C. Nicholson, Osteoblast-mediated effects on zinc on isolated rat osteoclasts: inhibition of bone resorption and enhancement of osteoclast number, Bone 19 (1996) 137–142.
[7] Y. Ramaswamy, C. Wu, H. Zhou, H. Zreiqat, Biological response of human bone cells to zinc-modified Ca–Si-based ceramics, Acta Biomater. 4 (2008) 1487–1497.
[8] C. Wu, Y. Ramaswamy, J. Chang, J. Woods, Y. Chen, H. Zreiqat, The effect of Zn contents on phase composition, chemical stability and cellular bioactivity in Zn–Ca–Si system ceramics, J. Biomed. Mater. Res. B: Appl. Biomater. 87 (2008) 346–353.
[9] A. Ito, K. Ojima, H. Naito, N. Ichinose, T. Tateishi, Preparation, solubility and cytocompatibility of zinc-releasing calcium phosphate ceramics, J. Biomed. Mater. Res. 50 (2000) 178–183.
[10] Y. Sogo, T. Sakurai, K. Onuma, A. Ito, The most appropriate (Ca + Zn)/P molar ratio to minimize the zinc content of ZnTCP/HAP ceramic used in the promotion of bone formation, J. Biomed. Mater. Res. 62 (2002) 457–463.
[11] A. Ito, H. Kawamura, M. Otsuka, M. Ikeuchi, H. Ohgushi, K. Ishikawa, et al., Zinc-releasing calcium phosphate for stimulating bone formation, Mater. Sci. Eng. C 22 (2002) 21–25.
[12] H. Kawamura, A. Ito, T. Muramatsu, S. Miyakawa, N. Ochiai, T. Tateishi, Long term implantation of zinc-releasing calcium phosphate ceramics in rabbit femora, J. Biomed. Mater. Res. A. 65 (2003) 468–474.

[13] T.J. Webster, C. Ergun, R.H. Doremus, R.W. Siegel, R. Bizios, Enhanced osteoclast-like cell functions on nanophase ceramics, Biomaterials 22 (2001) 1327.
[14] L. Zhang, T.J. Webster, Nanotechnology and nanomaterials: promises for improved tissue regeneration, Nano Today 4 (2009) 66.
[15] A. Oki, B. Parveen, S. Hossain, S. Adeniji, H. Donahue, Preparation and in vitro bioactivity of zinc containing sol–gel-derived bioglass materials, J. Biomed. Mater. Res. A 69 (2004) 216–221.
[16] W. Xia, J.J. Chang, Preparation and characterization of nano-bioactive-glasses (NBG) by a quick alkali-mediated (sol–gel) method, Mater. Lett. 61 (2007) 3251.
[17] A.M. El-Kady, A.F. Ali, M.M. Farag, Development, characterization, and *in vitro* bioactivity studies of sol–gel bioactive glass/poly(L-lactide) nanocomposite scaffolds, Mater. Sci. Eng. C. 30 (2010) 120.
[18] T. Kokubo, H.M. Kim, M. Kawashita, H. Takadama, T. Miyazaki, M. Uchida, T. Nakamura, Nucleation and growth of apatite on amorphous phases in simulated body fluid, Glastech. Ber. Sci. Technol. 73C1 (2000) 247.
[19] L.L. Hench, J.K. West, The sol–gel process, Chem. Rev. 90 (1990) 33–72.
[20] C.J. Brinker, G.W. Scherer, Sol–Gel Science, Academic Press, Inc, 1990.
[21] J. Zhong, D.C. Greenspan, Processing and Properties of Sol–Gel Bioactive Glasses, J. Biomed. Mater. Res. B: Appl. Biomater. 53 (2000) 694–701.
[22] C.J. Brinker, G.W. Scherer, The Physics and Chemistry of Sol–Gel Processing, Academic Press, Inc., San Diego, CA, USA, 1990.
[23] C.J. Brinker, G.W. Scherer, Sol–gel Science, Academic Press, Inc., 1990.
[24] D.M. Sanders, W.B. Person, Hench LL, Appl. Spectrosc. 28 (1974) 247.
[25] V. Aina, G. Malavasi, A. Fiorio Pla, L. Munaron, C. Morterra, Zinc-containing bioactive glasses: surface reactivity and behaviour towards endothelial cells, Acta Biomater. 5 (2009) 1211–1222.
[26] Ill Yong Kim, Giichiro Kawachi, Koichi Kikuta, Sung Baek Cho, Masanobu Kamitakahara, Chikara Ohtsuki, Preparation of bioactive spherical particles in the $CaO–SiO_2$ system through sol–gel processing under coexistence of poly(ethylene glycol), J. Eur. Ceram. Soc. 28 (2008) 1595.
[27] P.W. McMillan, Glass–Ceramics, Academic Press, London, 1964.
[28] K. Wallace, Design of novel bioactive glass compositions, University of Limerick, Ph.D., 2000.
[29] M. Sengupta, Development of a zinc-releasing bioactive glass and assessment of osteoblast adhesion to glass by examining integrin expression, Imperial College London, M.Sc., 2003.
[30] I. Izquierdo-Barba, A.J. Salinas, M.J. Vallet-Regí, Biomed, Mater Res. 47 (1999) 243.
[31] A. Oki, B. Parveen, S. Hossain, S. Adeniji, H.J. Donahue, Biomed. Mater. Res. 69A (2004) 216.
[32] M. Vallet-Regí, A.M. Romero, C.V. Ragel, R.Z.J. LeGeros, Biomed. Mater. Res. 44 (1999) 416.
[33] S. Lowell, J.E. Shields, M.A. Thomas, M. Thommes, Characterization of Porous Solids and Powders: Surface Area, Pore Size and Density, Particle Technology Series, vol. 16, Kluwer Academic Publishers, 2004.
[34] W. Neuman, M. Neuman, The Chemical Dynamics of Bone Mineral, University of Chicago Press, Chicago, 1958.
[35] M.M. Pereira, A.E. Clark, L.L. Hench, Calcium phosphate formation on sol–gel-derived bioactive glasses in vitro, J. Biomed. Mater. Res. 28 (1994) 693.